European Polymer Journal 242 (2026) 114440

Contents lists available at ScienceDirect

European Polymer Journal

journal homepage: www.elsevier.com/locate/europolj

Structural transformation and charge regulation of natural rubber-derived polymeric anticoagulants☆

Katarzyna Byś [a,*], Pablo M. Blanco [a,b], Krzysztof Fink [c], Mateusz Psurski [d], Honorata Zachary [d], Miroslav Štěpánek [a], Peter Košovan [a], Mariusz Uchman [a,*]

[a] Department of Physical and Macromolecular Chemistry, Faculty of Science, Charles University, Hlavova 2030, 128 40 Prague 2, Czech Republic
[b] Department of Physics, NTNU - Norwegian University of Science and Technology, NO-7491 Trondheim, Norway
[c] Laboratory of Biomedical Chemistry, Hirszfeld Institute of Immunology and Experimental Therapy, Polish Academy of Sciences, 53-114 Wrocław, Poland
[d] Laboratory of Experimental Anticancer Therapy, Hirszfeld Institute of Immunology and Experimental Therapy, Polish Academy of Sciences, Wrocław 53-114, Poland

ARTICLE INFO

Keywords:
Polyelectrolytes
Charge-regulation
Heparin-mimicking
Polymeric anticoagulant
Natural rubber-derived

ABSTRACT

Heparin-mimicking polyelectrolytes act as anticoagulants *in vivo* due to their highly negative charge and high charge density. Unlike heparin, these polymers can be structurally tailored to tune chain length, sulfation degree and binding affinity, thereby modulating their therapeutic action. Here, we present two such heparin-mimicking polyelectrolytes, derived from natural rubber as an inexpensive and readily available raw material. These polymers, sodium poly((sulfamate-carboxylate) isoprene) (PISC) and poly((amino-carboxylate) isoprene (PACIS), contain sulfonate groups, as well as weakly acidic and basic groups on adjacent carbons, which enable us to tune their net charge in the biological pH range, while maintaining solubility and anticoagulation activity. Moreover, their activity may be further optimized by adjusting chain length. To test this tunability, we prepared a set of PISC- and PACIS-based copolymers varying in chain length and dispersity by post-polymerization modification of *cis*-1,4-polyisoprene. We characterized their structure and functionalization degree using various methods, further analyzing with potentiometric titration and computer simulations how their net charge varies with pH and affects aggregation. Despite aggregation, all PISC- and PACIS-based copolymers displayed heparin-mimicking activity, measured as activated partial thromboplastin time, while remaining biocompatible. In this context, the longest-chain copolymers performed best, extending aPTT by more than threefold in comparison with the control at 3.8 μg/mL, while maintaining biocompatibility up to 100 μg/mL across various cell lines. These findings demonstrate that natural rubber-derived polyelectrolytes provide a promising alternative to heparin for antithrombotic therapy.

1. Introduction

Heparin is a linear zwitterionic glycosaminoglycan commonly used for its anticoagulant properties. On a global scale, this life-saving and -sustaining pharmaceutical drug prevents and treats thrombotic diseases responsible for tens of millions of deaths annually [1], including pulmonary embolism, the third most common cause of cardiovascular death. [2] Increased tendency for fibrin clot formation has also been associated with various cancers [3] and viral infections [4] leading to a high incidence of deaths due to thromboembolic events. However, heparin entails biological, pharmacokinetic and clinical limitations. [5,6] Although heparin is widely used in clinical settings, patients with heparin-induced thrombocytopenia [7] or heparin resistance [8,9] require other therapeutic approaches because heparin can trigger immune responses. For this reason, researchers have developed alternatives to this antithrombotic agent, including heparin-mimicking polymeric anticoagulants. [10–14].

Heparin-mimicking polymers can be structurally tailored to tune their chain length, sulfation degree and binding affinity, thereby modulating their blood compatibility and therapeutic action. [15,16] Owing to its highly negative charge density, heparin strongly interacts with proteins and enzymes of the coagulation cascade, [17] so mimicking heparin function requires preparing polymers with a highly negative charge. Many approaches have been tested with sulfated linear

☆ This article is part of a special issue entitled: 'AFPM' published in European Polymer Journal.

* Corresponding authors.
E-mail addresses: byk@natur.cuni.cz (K. Byś), uchman@natur.cuni.cz (M. Uchman).

https://doi.org/10.1016/j.eurpolymj.2025.114440
Received 11 August 2025; Received in revised form 11 November 2025; Accepted 4 December 2025
Available online 5 December 2025

polymers, copolymers, glycopolymers and ionomers, whose anticoagulation efficacy varies with their molecular weight and chemical composition. [18–23] Among the negatively charged polymers studied for this clinical application, polysulfonated polymers stand out for their design versatility and high anticoagulation efficacy.

The anticoagulant activity of polysulfonated polymers derives from their structural similarities to heparin. Structurally, heparin is composed of highly sulfated disaccharide chains which vary in length. Unfractionated heparins (UFH) consist of a mixture of longer and shorter heparin molecules and require frequent monitoring after administration, whereas low molecular weight heparins (LMWH) display a more predictable pharmacokinetics thanks to their uniform chains with 6–12 saccharide units. [24–26] Although fractionated heparins offer several advantages, including reduced risk of heparin-induced thrombocytopenia [27], controlled enzymatic or chemical degradation of UFH for LMWH production remains a complex and costly process.[28] Yet, despite differing in chain length, both UFH and LMWH share the fundamental anticoagulation mechanism. This mechanism stems from their highly negative charge, which is essential for their anticoagulant activity.[13,29,30].

Changes in the net charge of the macromolecule significantly influence its structural properties with direct consequences for their potential applications in complexation, drug delivery, or biochemistry.[31] In solution, the net charge of weak polyelectrolytes and zwitterionic macromolecules can be determined by combining molecular simulations with titration experiments.[32–34] Furthermore, polymer charge can be tuned by carefully selecting the monomer and adjusting the chain length. Therefore, we hypothesized that the negative net charge of heparin-mimicking copolymers and, thus, their anticoagulant activity may be optimized by adjusting their chain length and dispersity.

This study aims to identify the key structure–function relationship(s) of heparin-mimicking copolymers to optimize their anticoagulant activity. For these purposes, we introduced functional groups responsible for the anticoagulant activity of heparin to *cis*-1,4-polyisoprene because this versatile starting material can be sourced from natural rubber or synthesized through anionic polymerization for biomedical applications. By post-polymerization modification of *cis*-1,4-polyisoprene, involving stereospecific addition of chlorosulfonyl isocyanate and basic opening of the newly formed lactam ring, we prepared poly((sulfamate-carboxylate) isoprene) (PISC)[35,36] with a high-charge density. This modification was then followed by an acid-induced cleavage of sulfamate groups, yielding an amino-acid-resembling poly((amino-carboxylate)isoprene) (PACIS).[37–39] With various chain lengths and dispersity values, these PISC- and PACIS-based copolymers were examined by proton nuclear magnetic resonance (^{1}H NMR), Fourier Transform Infrared (FTIR) spectroscopy, and elemental and pH-dependent zeta-potential analysis, in addition to potentiometric titrations combined with molecular dynamics simulations. Complementing

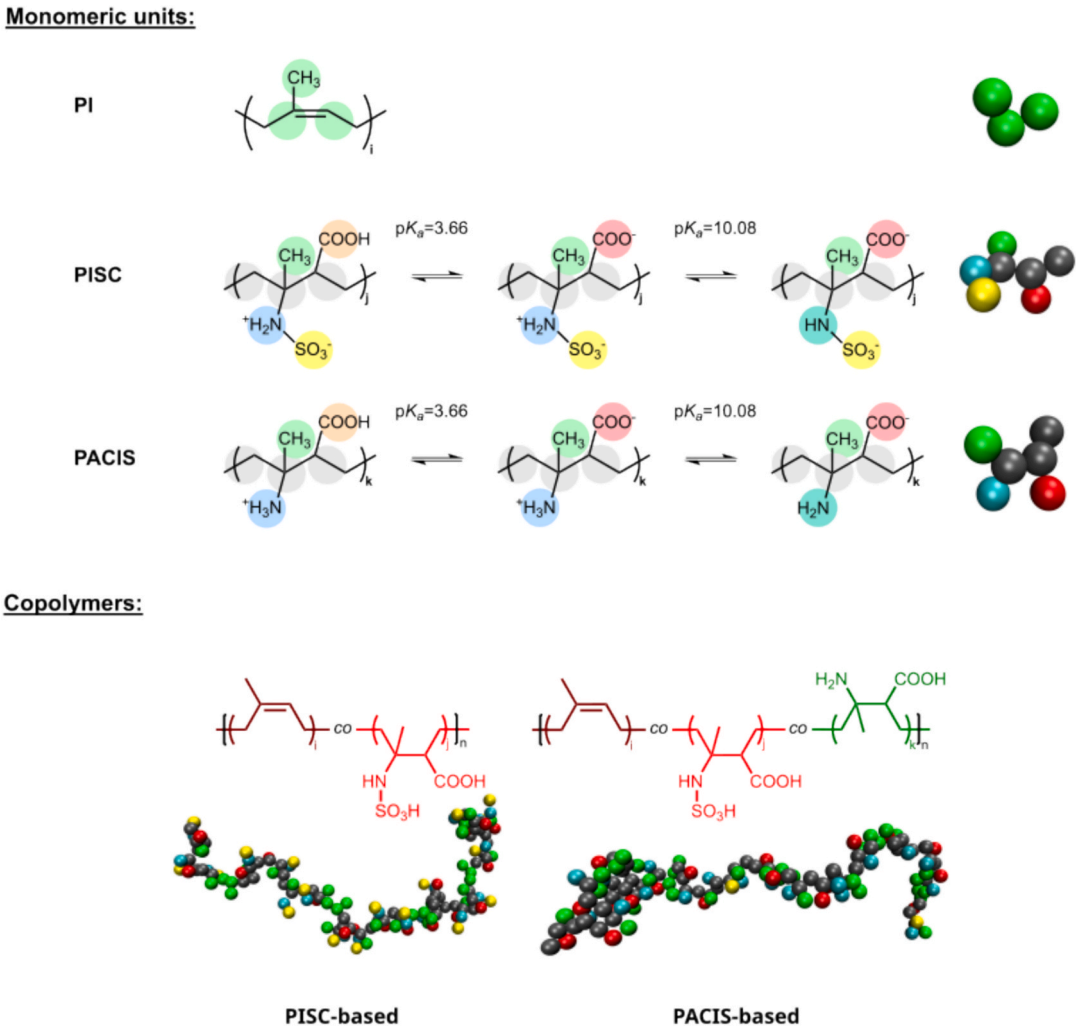

Scheme 1. Overview of the ionization states of poly((sulfamate-carboxylate) isoprene) (PISC) and poly((amino-carboxylate) isoprene) (PACIS), chemical structures of the PISC- and PACIS- copolymers with the simulation snapshots representing the coarse-grained model used for the corresponding copolymer. Color code: red, pink, yellow = acidic groups, blue, light blue = basic groups, grey = backbone groups, green = hydrophobic methyl groups.

this study, scattering experiments were performed at various pH values to examine structural changes at different ionization states (Scheme 1). Ultimately, the anticoagulant activity of PISC- and PACIS-based copolymers with various chain lengths and dispersities showed their impact on their biological activity.

2. Experimental part

2.1. Materials

Cis-1,4-polyisoprene, PI_NR ($M_w \sim 38$ kDa) was derived from natural rubber (Sigma-Aldrich), or synthesized by anionic polymerization – PI_7K and PI_75K ($M_w = 7.5$ kDa, $Đ$: 1.04 and $M_w = 75.5$ kDa, $Đ$: 1.08) (Polymer Source Inc.), chlorosulfonyl isocyanate (CSI) (98%; Sigma-Aldrich), 3-aminobutanoic acid (97%, Sigma-Aldrich), tetrahydrofuran (THF) (HPLC grade; Sigma-Aldrich), toluene (extra dry, 99.85%, VWR) were used as received from the suppliers. MilliQ (18.2 MΩ) water was used to prepare aqueous solutions. NMR, light scattering and small angle X-ray scattering solutions were prepared using deuterium chloride (DCl) (20% in deuterium oxide (D_2O); Chemotrade), sodium deuteroxide (NaOD) (30 wt% in D_2O, 99 atom% D, Sigma-Aldrich) and D_2O (99.9 atom% D; Sigma-Aldrich) solutions.

2.2. Methods

2.2.1. Polyelectrolyte synthesis

Poly(sulfamate-carboxylate isoprene) (PISC) was prepared by post-polymerization modification of *cis*-1,4-polyisoprene (PI) through a reaction of its C=C double bonds with chlorosulfonyl isocyanate, followed by alkaline hydrolysis of the lactam intermediate with NaOH. For this synthesis, a 250 mL flame-dried round-bottom flask was charged with 1 g (0.0263 mmol) of PI and 30 mL of extra dry toluene. The solution was stirred under an inert gas atmosphere until homogenous and subsequently cooled in an ice bath to 0 °C. Then, 3.18 mL (1.5 equivalent excess of PI double bonds) of chlorosulfonyl isocyanate was added dropwise over 30 min under constant and vigorous stirring. After this period, the solution was stirred overnight under an Ar atmosphere before evaporating the solvent under reduced pressure. The whiteish intermediate product was isolated by repeated washing with diethyl ether followed by filtration. The lactam intermediate was transferred to a 100 mL round-bottom flask along with 50 mL of a 1 M NaOH solution in a water/methanol mixture (water/methanol; v/v 1:3). The reaction mixture was left to reflux for 24 h at 85 °C. After 3 h, the solid lactam intermediate became soluble, indicating opening of the lactam ring. The brown solution was then brought to room temperature, and methanol was evaporated under reduced pressure. The remaining solution was dialyzed against double-distilled water using dialysis membranes with a molecular weight cut-off of 3.5 kDa. Dialysis was performed until the complete removal of NaOH, as confirmed by pH measurements. Lastly, the white powder was isolated from the aqueous solution by lyophilization. Yield: 79%.

2.2.2. Acid-induced sulfamate cleavage

Poly((amino-carboxylate) isoprene) (PACIS) was synthesized by acid-induced cleavage of PISC sulfamate groups. For this purpose, 170 mg of PISC was dissolved in 21.25 mL THF, and 85 mL 0.1 M HCl (THF/HCl v:v 1:4) was added dropwise. The solution was then stirred for 4 h at 70 ℃. After the reaction, the mixture was cooled to room temperature and dialyzed for 24 h against 0.1 M HCl (MWCO = 3.5 kDa) and for another 24 h against double-distilled water. The powder was isolated from the aqueous solution by lyophilization. Yield: 82%.

2.2.3. Nuclear magnetic resonance spectroscopy (NMR)

^{1}H NMR spectra were measured on a 400 MHz Bruker Avance III spectrometer using deuterium oxide or deuterated THF as solvents. The solvent residual peak of the respective solvent was used as a standard. All measurements were conducted at 298.15 K. The data was processed using MestReNova software.

2.2.4. Elemental analysis

Elemental analysis of C, H, N, and S was performed on a PerkinElmer 2400 series II CHN analyzer.

2.2.5. Fourier transform infrared spectroscopy (FTIR)

FTIR spectra of samples were recorded on a Thermo Fisher Scientific Nicolet iS50 FTIR spectrometer (4 cm^{-1} resolution, Happ-Genzel apodization) in the 400–4000 cm^{-1} (KBr beamsplitter) region, 64 scans, using DRIFT and ATR (diamond crystal) technique. Standard ATR correction was applied to the recorded spectra.

2.2.6. Size exclusion chromatography (SEC)

Polymer molecular weight and dispersity ($Đ = M_w/M_n$) were determined by SEC in THF on an Agilent Technologies 1260 infinity Series apparatus fitted with a UV/vis Diode Array Detector (DAD) and a Differential Refractometer at an elution flow rate of 0.7 mL/min. The system was equipped with three PL-gel (polystyrene-divinylbenzene) columns (Mixed B, Mixed C, and Mixed D, Polymer Laboratories, UK) calibrated using a set of polystyrene (PS) standards (Polymer Laboratories, UK). For characterization, approximately 6 mg of the sample was dissolved in THF and filtered through a 0.45 μm PVDF membrane syringe filter into a chromatography vial equipped with a screw cap with a septum. The data were processed in Clarity software.

2.2.7. Static and dynamic light scattering

DLS and SLS measurements were simultaneously performed on an ALV light scattering photometer (ALV, Germany), equipped with an ALV CGS-3 automatic goniometer, an ALV 7004 Multiple-Tau digital correlator, a Cobolt Flamenco diode-pumped solid state laser ($\lambda = 660$ nm, $P = 100$ mW) (Hübner Photonics, Germany), and two high-QE avalanche photodiode pseudo cross-correlation detectors (Excelitas Technologies, USA). The measurements were performed for scattering angles ranging from 50° to 130° with an angular step of 10°, at 23 °C. The resulting scattering vectors, $q = \frac{4\pi n_0}{\lambda}\sin\frac{\theta}{2}$ (n_0 is the solvent refractive index) ranged from 10.7 to 23.0 μm^{-1}. The instrument setup was equipped with a cell housing system containing toluene, which was used as an index-matching fluid. The samples were prepared by dissolution in D_2O at a concentration of 5 g/L. Deuterium oxide was used as a solvent as the samples were then used in NMR measurements. DLS measurements were evaluated by fitting the measured normalized time autocorrelation function of the scattered light intensity, $g^{(2)}(t,q)$, related to the electric field autocorrelation function, $g^{(1)}(t,q)$, using the Siegert relation, $g^{(2)}(t,q) = 1 + \beta|g^{(1)}(t,q)|^2$, where β is the coherence factor. The data were fitted using the constrained regularization algorithm (CONTIN), which provides the distribution of relaxation times τ, $A(\tau,q)$ as the inverse Laplace transform of $g^{(1)}(t,q)$ function. The $A(\tau,q)$ distributions can be recalculated to the distributions of the apparent hydrodynamic radii, R_h^{app}, using the relationship, $R_h^{app} = \frac{k_B T q^2 \tau}{6\pi\eta}$, where k_B stands for the Boltzmann constant; T, for the temperature; and η, for solvent viscosity.

2.2.8. Small-angle X-ray scattering

Small-angle X-ray scattering (SAXS) measurements were performed at BIOCEV (Vestec, Czech Republic) on a SAXSpoint 2.0 (Anton Paar, Austria) instrument equipped with a MetalJetC2 + X-ray source containing a liquid gallium alloy anode ($\lambda = 0.134$ nm) and an EIGER R 1 M Horizontal detector. The samples were loaded into a 1-mm quartz capillary either using a high-precision low-volume auto-sampler with temperature control or manually. The sample-to-detector distance was 0.78 m, which corresponds to the q vector range ($q = \frac{4\pi}{\lambda}\sin\frac{\theta}{2}$) from 0.047 to 4.4 nm^{-1}. Constructing SAXS curves required azimuthal-averaging scattering patterns for both samples and solvents. At a concentration of 5 g/L, polymer samples were prepared in D_2O (salt

concentration: 0.1 M) – samples denoted as N, a 0.1 M solution of NaOD in D_2O – samples denoted as B and a 0.1 M solution of DCl in D_2O – samples denoted as A. The measurements were performed at 25 °C.

2.2.9. Zeta potential measurements

The zeta potential (ζ) measurements were performed on a Malvern Zetasizer Ultra (Malvern Panalytical, United Kingdom) equipped with a 633-nm He/Ne gas laser and with an avalanche photodiode. Each sample was placed into a standard polystyrene cuvette equipped with a Universal 'Dip' Cell Kit (ZEN1002, Malvern Panalytical, United Kingdom). The values of ζ-potential were averaged from 3 measurements. The ζ-potential values were calculated from the electrophoretic mobilities using the Henry equation in the Smoluchowski approximation, $\mu = \epsilon\zeta\eta$, where μ stands for the electrophoretic mobility; η, for the solvent viscosity, and ϵ, for the dielectric constant of the solvent. The samples of each polymer were prepared at an initial concentration of 1 g/L in 0.1 M HCl. The pH of the samples was adjusted to either 0.2 or 1 pH point intervals using a Metrohm 888 Titrando Compact titrator equipped with a magnetic stirrer, a Pt1000 temperature sensor, and an LL Biotrode 3.0 mm glass electrode.

2.2.10. Potentiometric titration

Potentiometric titrations of PISC and PACIS were performed on a Metrohm 888 Titrando Compact titrator equipped with a Metrohm LL Biotrode 3-mm glass electrode, a Pt1000 temperature sensor, and a magnetic stirrer. Used for sample preparation and titration, standardized HCl and NaOH stock solutions from Carl Roth GmbH (Karlsruhe, Germany) were kept under soda lime before measurements to prevent CO_2 absorption and ensure their accuracy. All polyzwitterions were dissolved in a standardized 0.1 M HCl solution and titrated using standardized 0.1 M NaOH with an initial titrate volume of 2.0 mL. The titrations were performed until reaching a pH of 12.0. All measurements were preceded by a blank sample measurement, which consisted of titrating 2.0 mL of a 0.1 M HCl solution under the same conditions. The measurements were performed at 23 °C.

2.2.11. Simulation model and method

Computer simulations were performed using bead-spring coarse-grained models of different polymers to study their charge regulation. The model is only briefly described here and additional details are provided in Supporting Information (SI) in Section S3. Each simulation included one polymer chain with $N_m = 24$ monomers and explicit monovalent salt ions. The concentration of added salt was 0.1 M, corresponding to the ionic strength of the solutions used for the potentiometric titration.

The polymer chains were statistical copolymers with PISC, PACIS and PI monomeric units. As shown in Scheme 1, each monomeric unit included several beads, each of them encapsulating one functional group. For simplicity, all particles in the system had the same size, $\sigma = 0.335$ nm. The model included Lennard-Jones interactions, accounting for steric hindrance and hydrophobicity, electrostatic interactions and acid-base equilibria of carboxyl and amino groups. Commonly applied in polymer science, similar coarse-grained models have been used in our previous studies on charge regulation of various weak polyelectrolytes, including polyzwitterions, as those studied here[40].

The system was simulated using a combined Langevin Dynamics and constant-pH Monte Carlo [34] (cpH) scheme to sample both configuration and ionization states, respectively. The cpH trial moves involved altering the protonation state of amino and carboxyl beads, thereby changing their charge to mimic the following chemical reactions:

$$COOH \leftrightarrow COO^- + H^+ \tag{2}$$

$$NH_3^+ \leftrightarrow NH_2 + H^+ \tag{3}$$

Electroneutrality was maintained by inserting/deleting a neutralizing small cation. These cpH trial moves were accepted with a probability which depends on the interaction energy, on the pH, and on the intrinsic pK_a of the functional groups. The last two served as critical inputs for the simulation. The excess chemical potential of the neutralizing cation was corrected *a posteriori*, following the procedure explained in Ref. [41].

The sulfonate groups in PISC monomeric units were deemed permanently negatively charged, given their low pK_a value. The pK_a values for carboxyl and amino groups were estimated so as to reproduce the potentiometric titration of 3-aminobutanoic acid (cf. Section 3.2), measuring intrinsic pK_a values of 3.66 and 10.08, respectively. Further details on how these pK_a values were estimated from potentiometric data are available in SI (Section S3). We chose 3-aminobutanoic acid to calibrate our cpH simulations because its chemical structure closely resembles the monomeric unit of PACIS (See Scheme 1). Therefore, the intrinsic pK_a values of amino and carboxylic groups in 3-aminobutanoic acid should be similar to those of the same groups in PACIS and PISC copolymers.

The direct output of the simulations was the average degree of ionization of each group α_i used to calculate the net charge per effective monomer

$$Z_m^{eff} = \frac{e}{N_m}\sum_{i=1}^{N_m}\alpha_i z_i \tag{4}$$

where $z_i = -1$ for an acid, $z_i = +1$ for a base, and e is the elementary charge. The chain length, N_m, counts for all monomeric units of the polymer, including the neutral PI units. Therefore, Z_m^{eff} should be understood as an effective net charge over all monomer units, as explained in SI (Section S5). All simulations were run in ESPResSo v4.2.2 [42] using pyMBE v0.8.0 [43]. This Python-based molecule builder made it easier to setup the model of highly heterogeneous copolymers.

2.2.12. Biocompatibility study and cell culture

Cell proliferation inhibition was tested in four cell lines (MDA-MB-231, CAL-51, CAL-148 and MV-4–11). CAL-51 and CAL-148 cell lines were purchased from the Leibniz Institute DSMZ-German Collection of Microorganisms and Cell Culture (DSMZ, Braunschweig, Germany). MDA-MB-231 and MV-4–11 cell lines were purchased from the American Type Culture Collection (ATCC Rockville, MD, USA). These cell lines were maintained at the Hirszfeld Institute of Immunology and Experimental Therapy (HIIET) and tested for mycoplasma contamination using VenorGeM Classic (Minerva Biolabs, Berlin, Germany), with negative results in all cases.

CAL-51 and CAL-148 cells were cultured in high-glucose DMEM medium (Biowest, Nuaillé, France) supplemented with 10% (v/v) fetal bovine serum (FBS), GE Healthcare HyClone, Logan, UT, USA) and 2 mM L-glutamine (Sigma Aldrich, Poznan, Poland). CAL-148 culture medium was additionally supplemented with 20 ng/mL human EGF (Sigma Aldrich, Poznan, Poland). HEK-293 (an immortalized epithelial cell line derived from human embryonic kidney cells) and CCD-841 (colonocytes from healthy donor) were purchased in ATCC and cultured in Eagle's Minimum Essential Medium (Life-Technologies) supplemented with 10% FBS. MDA-MB-231 and MV-4–11 cells were cultured in RPMI-1640 (Biowest, Nuaillé, France) supplemented with 10% (*v/v*) FBS and 2 mM L-glutamine. MV-4–11 medium was additionally supplemented with 1 mM sodium pyruvate (Sigma Aldrich, Poznan, Poland. All culture media contained antibiotics, namely 100 U/mL penicillin and 100 mg/mL streptomycin (both Polfa-Tarchomin, Warsaw, Poland). In all experiments, all cell lines were cultured in an incubator with a humid atmosphere at 37 °C and 5% (*v/v*) CO_2 and passaged twice a week using EDTA-Trypsin (pH 8; HIIET, Wroclaw, Poland) solution as a detachment agent for adherent cell lines only. Cisplatin was used as a ready-to-use, 1 mg/mL stock solution, stored at room temperature (Ebewe, Austria).

For the antiproliferative test, cells were seeded on 384-well plates (10^3 cells/well; Greiner BIOScience). After 24 h, the cells were treated

with polymer solutions at seven concentrations (starting concentration 316 μg/mL; 3.16 × dilution factor). After 72 h, cell growth inhibition was assessed using the MTT [44] (for Cal-148 and MV-4–11) or SRB [45] (for Cal-51, MDA-MB-231, HEK-293, and CCD-841) assays with minor modifications to adapt the original protocol to 384-well plates format. Each compounds/ concentration was tested in triplicate, in a single experiment, and each experiment was repeated at least three times independently. Results are expressed as cell growth inhibition (%) ± SD ($n = 3$) calculated using the following formula:

$$Growthinhibition(\%) = \left[100 \times \left(1 - \frac{A_t - A_m}{A_c - A_m}\right)\right] \quad (5)$$

where A_t stands for absorbance of compound-treated wells; A_c, for absorbance of control, vehicle-treated wells; and A_m, for absorbance of blank (medium) wells

If possible, the IC50 value (concentration at which a compound reduces cell growth by 50%) was calculated in GraphPad Prism 7.2 software using (Inhibitor) vs. response – variable slope (four parameters) model (Hill's equation).

The potential cell growth stimulation at polymers' low concentration was evaluated by fitting the data to the 4-parameter Hill's equation, followed by an extra sum-of-squares F test on the bottom parameter (deviation from zero); results with $p < 0.05$ were deemed significantly different.

After 72 h of treatment, HEK-293 cells images were acquired under an Opta-tech MW50 microscope equipped with an Mi20 camera in brightfield mode.

2.2.13. Anticoagulation study

To assess the antithrombotic properties of the polymers, basic coagulation studies were performed using the following Bio-Ksel reagents (Grudziądz, Poland): activated partial thromboplastin time (aPTT) reagent, calcium chloride, and lyophilized normal plasma. The aPTT reagent acts as an activator and stimulates the production of XIIa factor. To measure 100 μL of rehydrated plasma, 100 μL of aPTT reagent was added to a vial and incubated at 37 °C for 180 s. To the activated solution, 100 μL of calcium chloride was added, causing the formation of a stable fibrin clot. Polymer samples additionally contained 25 μL of a buffered polymer solution at concentrations of 1000, 500, 100, 50, 10, and 5 μg/mL. aPTT was optically determined by measuring the time between the addition of $CaCl_2$ and the formation of a clot in relation to the thrombotic time of a blank. The aPTT was expressed as a percentage of the vehicle (buffer-treated control) ± SD (n = 3).

2.2.14. Hemolytic assay

The hemolytic activity of the compounds was evaluated as the amount of hemoglobin released by disrupting human red blood cells (hRBCs), also known as erythrocytes. hRBCs were collected by centrifugation at 1,500 g for 15 min, washed two times with PBS (10 mM, pH 7.4) and suspended to a final concentration of 5% v/v. Then, an equal volume of erythrocyte suspension and compound solution at various concentrations was mixed in 96-well plates and incubated for 1 h at 37 °C. After centrifugation at 1,000 g for 5 min, the absorbance of the supernatant was measured at 490 nm to monitor hemoglobin release on a microplate reader (Biotek Synergy H4 Hybrid Reader). Erythrocytes treated and untreated with 1% Triton X-100 were used as positive and negative controls, respectively. The hemolysis percentage was calculated using the following equation:

$$Hemolysisrate(\%) = \frac{A(\text{compounds}) - A(\text{negative control})}{A(\text{positive control}) - A(\text{negative control})} \times 100\% \quad (6)$$

The half-maximal effective concentration (EC_{50}) was defined as the concentration at which the compound caused 50% hemolysis. The experiments were performed in triplicate.

2.2.15. Differential scanning calorimetry (DSC)

The thermal properties were analyzed on a Mettler Toledo type 822e differential scanning calorimeter (DSC) (Mettler Toledo, Columbus, OH, USA), operated with Stare System software 16.20. Heating was conducted at a rate of 10 °C/min. Aluminum crucibles containing samples weighing 0.015 g were placed into the measurement chamber. Measurements were performed in a nitrogen atmosphere at a flow rate of 60 cm^3/min, covering a temperature range from −95 to 200 °C for PI, from −135 to 220 °C for PISC and from 5 to 200 °C for PACIS.

2.2.16. Thermogravimetric analysis (TGA)

Thermogravimetric analysis (TGA) was performed on a Pyris 1 TGA thermogravimetric analyzer (from Perkin Elmer, Waltham, MA, USA) in a temperature range from 30 to 800 °C, at the heating rate of 10 °C/min. All analyses were performed in nitrogen and in air.

3. Results and discussion

3.1. Synthesis and characterization of PISC and PACIS polyelectrolytes

All polyelectrolytes were synthesized from the precursor polymer *cis*-1,4-polyisoprene (PI). PI was either derived from natural rubber (PI_NR) or synthesized by living anionic polymerization using organolithium initiators (PI_7K, PI_75K). The origin of the PI sample strongly affects polymer dispersity: PI polymers sourced from natural rubber have a $Đ \approx 3.15$, whereas anionically polymerized PI polymers are fairly homogeneous in size, with a $Đ$ below 1.1. The composition of both the initial PI polymers and the resulting copolymers is outlined in Table 1.

The thermal stability of the starting PI polymers increased with their chain length. The thermal decomposition profile of both synthetic (PI_7K, PI_75K) and natural (PI_NR) polyisoprenes showed polymer decomposition (Fig. S1B). This decomposition most likely resulted from random chain scission and depolymerization, as observed in natural rubber between 300 and 500 ℃. [46].

All polyisoprenes decomposed when heated to 400 °C, as expected for PI polymers (Fig. S1B). However, the shorter polyisoprene chains were less thermally stable than their longer counterparts, resulting in a broadened decomposition range. The shorter chains were less entangled, which lowered the activation energy of chain scission and degradation.

The polyelectrolytes were synthesized by post-polymerization of PI_NR, PI_7K and PI_75K (Fig. 1A). The first step included a stereospecific addition of chlorosulfonyl isocyanate (CSI) to PI at 0 ℃ in anhydrous toluene, yielding a β-lactam intermediate. In an NaOH-mediated reaction, the lactam ring was opened, producing the PISC-based copolymer. This reaction with CSI was stereospecific, proceeding only with the *cis*-PI, so the polymer chain was functionalized to an extent corresponding to the *cis*-isomer content in the initial polymer (Table 1, Fig. S1A). Therefore, the modified PISC consisted of high-charge density monomeric units. Each unit contained two negatively charged groups with different pH-sensitivity. The high content of sulfamate groups, which are negatively charged over a broad range of pH, ensures the anticoagulant activity of this copolymer.[47].

The second step of the reaction, that is, acid-induced cleavage of the sulfamate group at 70 °C, yielded the poly(amino-acid)-mimicking PACIS-based copolymer. Poly(amino-acids) are known for interacting with cellular membranes and modulating immune responses.[48] Based on elemental analysis, 90% N-S bonds were cleaved under our reaction conditions (Section S2 in the Supporting Information). As a result, the PACIS-based copolymer contained small fractions of unmodified PISC and PI units (Table 1), which were also present in PISC-based copolymers. The structural and functional implications of these residual units are discussed below (Figs. 2 and 3).

To monitor the progress of these reactions, we characterized the products by ^{1}H NMR, FTIR, TGA and DSC. Fig. 1B shows the ^{1}H NMR spectra of the starting PI (brown), PISC-based copolymer (red) and PACIS-based copolymer (green). The spectrum of PI illustrates the

Table 1
Molecular characterization of the starting PI polymers and modified PISC- and PACIS-based copolymers, i, j, k – molar fraction of PI, PISC, and PACIS units, respectively.

STARTING POLYMERS						MODIFIED COPOLYMERS			
	M_n (kDa)	M_w (kDa)	dispersity (Đ)	% *cis*-1,4[c]	n PI		i PI	j PISC	k PACIS[d]
PI_NR	111[a]	40.4[a]	3.6[a]	97	1629	PISC NR	0.16	0.84	–
						PACIS NR	0.16	0.18	0.66
PI_7K	7.2[b]	7.5[b]	1.04[b]	82	105	PISC 7 K	0.18	0.82	–
						PACIS 7 K	0.18	0.10	0.72
PI_75K	70[b]	75.5[b]	1.08[b]	80	1027	PISC 75 K	0.25	0.75	–
						PACIS 75 K	0.25	0.17	0.58

[a] SEC analysis was performed in THF on a Varian liquid chromatograph equipped with refractive and UV light scattering detectors. Three SEC columns from Supelco (G6000-4000–2000 HXL) were used with triple detectors from Viscotek Co.
[b] Data retrieved from the manufacturer's characterization sheet.
[c] From ^{1}H NMR in THF-d8, 400 MHz.
[d] From elemental analysis.

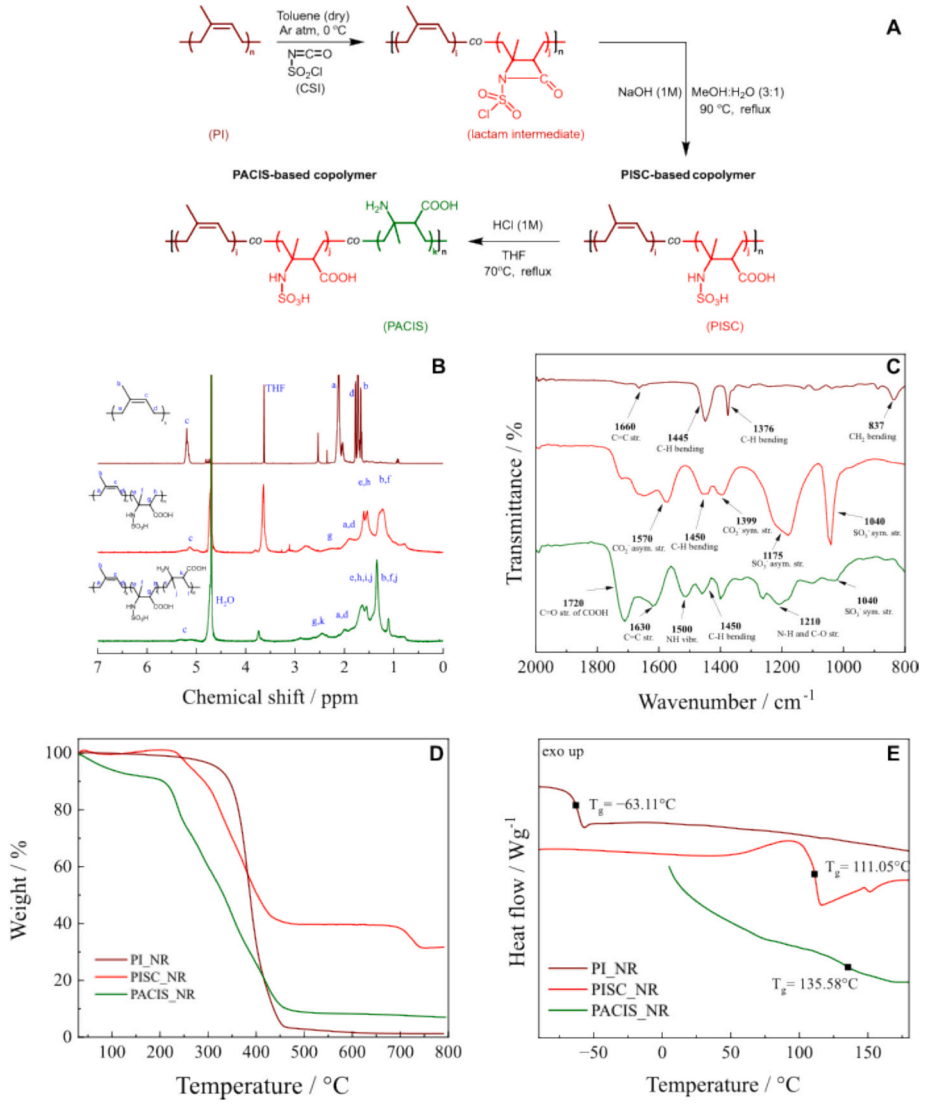

Fig. 1. Post-polymerization of polyisoprene (PI) into PISC- and PACIS-based polymers. **(A)** Overview of the synthesis pathway **(B)** ^{1}H NMR (THF-d8, 400 MHz or D_2O, 400 MHz) and **(C)** FTIR spectra and **(D)** thermogravimetric analysis (TGA) and **(E)** differential scanning calorimetry (DSC) curves of PI_NR, PISC_NR and PACIS_NR.

characteristic signals of the *cis*-isomer, including the peak corresponding to the vinyl (5.2 ppm) and aliphatic backbone protons. Upon chlorosulfonyl isocyanate addition and lactam ring opening, the resulting spectrum of the PISC-based copolymer displays a significantly smaller peak corresponding to the vinyl protons. By comparing the integral of this peak with that of the protons of the methyl group attached to the substituted carbon, we confirmed the extent of the reaction. The results showed a successful modification, with approximately 82, 84, and 75%

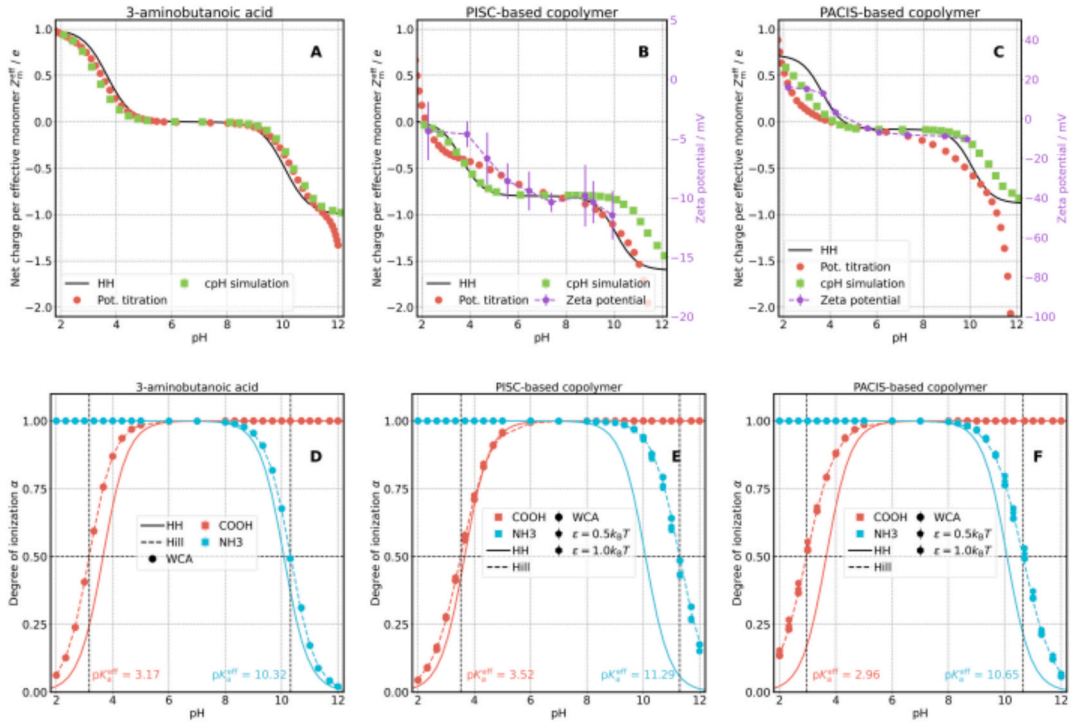

Fig. 2. Top panel: net charge per effective monomer Z_m^{eff} as a function of pH for the following samples: (A) 3-aminobutanoic acid, (B) the PISC-based copolymer and (C) the PACIS-based copolymer. Z_m^{eff} was estimated by potentiometric titration (circles, Pot. titration), constant-pH molecular simulations (squares, cpH simulation), and zeta potential measurements (pentagons). The ideal baseline is given by the Henderson Hasselbach (HH) equation (Eqs. 1 and 4), calculated with the input pK_a values used for the cpH simulations. Bottom panel: Degree of ionization as a function of pH measured with constant pH Monte Carlo simulation (cpH) for the following systems: (D) 3-aminobutanoic acid, (E) the PISC-based copolymer and (F) the PACIS-based copolymer. Symbol shape encodes cpH simulations performed with different non-bonded interaction potentials: the purely repulsive Weeks-Chandler-Andersen (WCA) potential (circles), and the Lennard-Jones potential with different potential wells $\varepsilon = 0.5k_BT$.

of the monomeric units of PI_7K, PI_NR, and PI_75K, respectively, being converted into their corresponding PISC forms. The spectrum of the PACIS-based copolymer shows broad overlapping peaks of the final product and PISC-based copolymer residues. We confirmed this cleavage by FTIR analysis. In the FTIR spectrum of PISC_NR, the strong bands at 1175 and 1040 cm^{-1} correspond to $-SO_3^-$ stretching, confirming CSI addition, while the peaks at 1399 and 1570 cm^{-1} correspond to $-CO_2-$ stretching in –COOH (Fig. 1C), demonstrating that PISC was synthesized successfully. In turn, the PACIS-based copolymer was prepared by acid-induced cleavage of sulfamate groups, as evidenced by the decrease of the $-SO_3^-$ stretching bands (1040 cm^{-1}) in the FTIR spectra (Fig. 1C). The extent of the conversion of PISC-based copolymers into PACIS-based copolymers was quantitatively evaluated by elemental analysis. In agreement with the FTIR results, elemental analysis indicated partial cleavage of the sulfamate bonds. The degree of the this cleavage was determined from the difference in sulfur content between PISC- and PACIS-based copolymers, Based on these results, sulfamate bond cleavage reached 87.5, 78.2, and 77.1% for PACIS_7K, PACIS_NR, and PACIS_75K, respectively.

In Fig. 1D, the thermal degradation profile of the PISC-based copolymer shows a significant decrease in the percentage of mass loss between 300 and 450 ℃. In addition to chain scission, mass loss may also result from functional group decomposition, i.e., S-O or S-N bond cleavage, and the ensuing formation of sulfuric compounds, such as sulfur dioxide and trioxide, in trace amounts.[49] Sulfur- and nitrogen-rich residues often contribute to char stabilization by forming heteroatom-conjugated structures. Along with the stable carbonaceous residue from the polymer chain, these structures may explain the significant char content observed between 450 and 700℃. Moreover, crosslinking between double bonds in the PISC-based copolymer may further stabilize the material at high temperatures.[50].

The starting PI and the PISC- and PACIS-based copolymers showed distinct glass transition temperatures (T_g) at 63.1, 111.05 and 135.58 ℃, respectively, further confirming their modifications (Fig. 1E). Reaching 15.07 and 13.42% mass loss after the first heating run in the DSC analysis, both PISC- and PACIS-based copolymers, respectively, proved hygroscopic (Fig. 1E). Therefore, the water content and composition of these copolymers must be determined accurately because even small amounts of water may affect their titrations.

3.2. pH response of the PISC- and PACIS-based copolymers

Our heparin-mimicking co-polymers have weak acid and basic groups and therefore their net charge is pH-sensitive. Such changes in net charge could have important implications for the anticoagulant properties of our copolymers. To characterize the response of the net charge of the copolymers to pH variations, we combined experimental measurements (potentiometric titrations and zeta potential) and constant pH simulation (cpH), presented in Fig. 2. Each method comes with its own advantages and limitations and, therefore, brings different insights.

The experimental measurements provide direct evidence from the copolymer samples. However, the raw data from potentiometric titration is the pH as a function of added titrant (Section S5 in Supporting Information). The concentration of all species in solution must be known with analytical precision to reliably calculate the net charge of the co-polymers from such raw data, which is a challenging task for the poly-disperse solutions studied here. The net charge of the copolymers can be indirectly inferred from zeta-potential measurements, but there is no well-defined relation between the zeta-potential and the net charge of the copolymers in solution. The zeta potential measures the electro-phoretic mobility of the macromolecules in solution, which is

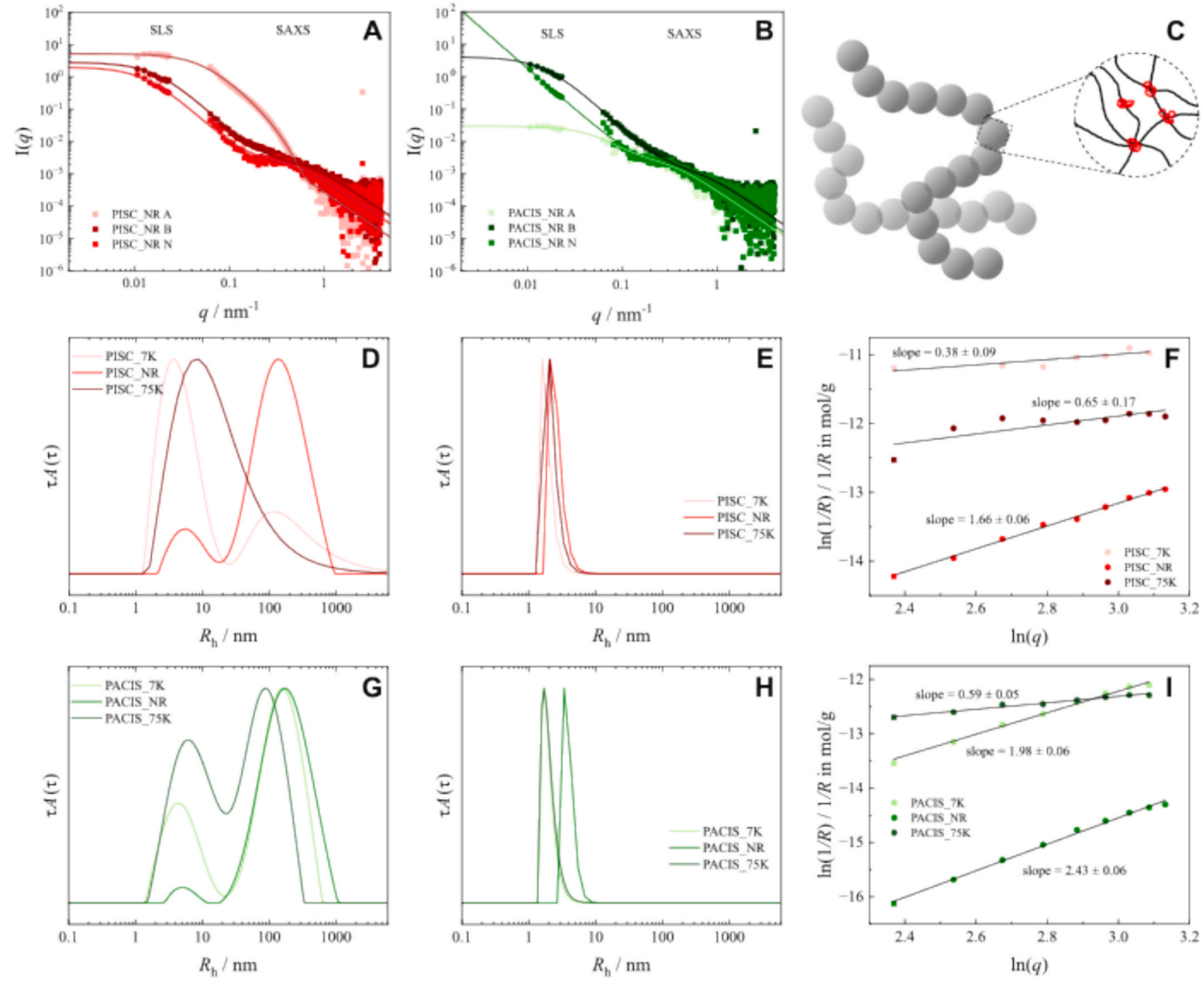

Fig. 3. PISC- and PACIS-based copolymers form fractal aggregates in solution. At the top: Static light (SLS) and small-angle X-ray (SAXS) scattering of PISC_NR- **(A)** and PACIS_NR-based **(B)** copolymers at constant ionic strength (0.1 M) and acidic (_A), basic (_B), and neutral (_N) solution pH. **(C)** Schematic representation of the fractal aggregate with hydrophobic domains (red). Dynamic Light Scattering (DLS) of the PISC- (**(D)** intensity- and **(E)** number-weighted hydrodynamic radius distribution) and PACIS-based copolymers (**(G)** intensity- and **(H)** number-weighted hydrodynamic radius distribution). Static Light Scattering, ln(q) as a function of ln(1/R) of PISC- **(F)** and PACIS-based copolymers **(I)** with three different chain lengths. (To interpret the references to color in this figure legend, the reader should refer to the web version of this article.)

determined by their surface charge. This parameter can be significantly different from their net charge, especially if the macromolecules aggregate or contain both cationic and anionic groups with complex spatial distribution. Aggregation likely affects the zeta potential and potentiometric titrations, albeit in different ways. The primary quantity measured by the zeta sizer is electrophoretic mobility, which is then used to calculate the zeta potential. Mobility mostly depends on the surface charge, whereas charges buried deeper in the aggregate contribute less. On the contrary, potentiometric titrations determine the net charge (bare charge) of the polymers, which is calculated from the electroneutrality requirement and from the known amounts of small ions. Here, all charges on the sample contribute equally, whether they are on the surface or not. Thus, aggregating polymers may display a different trend in the variation of pH as a function of the zeta potential and net charge determined from potentiometric titrations. [32,34] cpH simulations offer a well-defined system to directly sample the net charge of the copolymers, but their accuracy depends on how well the chosen simulation model captures the physicochemical properties of the copolymers. Our model features a single copolymer chain including electrostatics and two different models for intrachain interactions: the purely steric Weeks-Chandler-Andersen (WCA) potential and the Lennard Jones (LJ) potential, including hydrophobicity. In the following, all results from cpH simulations use the WCA model unless otherwise stated. By combining the cpH simulations with experimental measurements, we overcome the limitations of each method by cross-validating the results measured from each independent method.

First, we calibrated our molecular simulations to reproduce the potentiometric titration measurements for the simple case of a dilute solution of 3-aminobutanoic acid (Fig. 2). The chemical structure of 3-aminobutanoic acid closely resembles the monomeric unit of PACIS, thereby providing a reasonable approximation for the intrinsic pK_a values of carboxylic and amino groups in PISC and PACIS copolymers. The potentiometric titration data closely follows the Hendersson Hasselbach (HH) equation:

$$\alpha^{-1} = 1 + 10^{z(pH-pK_a)} \tag{7}$$

Where α is the degree of ionization, with $z = 1$ for acidic groups and $z = -1$ for basic groups. To estimate the intrinsic pK_a values of 3-aminobutanoic acid, we fitted the potentiometric titration data to the Hendersson Hasselbach (HH) equation, corrected by the activity coefficient of the salt ions (Eq. S11-S12). The fitting yielded intrinsic pK_a values of 3.66 and 10.08 for the carboxylic acid and amino groups, respectively. Then, we performed a simulation with the estimated values as inputs to verify that our calibration was correct. Fig. 2A shows that our simulations mirrored the experimental titration results, demonstrating that the calibration worked well. The small deviations from the ideal HH result derived from the ionic strength, which affects the activity coefficients of the ions.[51] Therefore, we used these pK_a values as input of our cpH simulations of PISC and PACIS-based copolymers.

To characterize the pH-responsive ionization of these polymers, we calculated the net charge per effective monomer Z_m^{eff} at different pH values from the simulations and from different experiments (Fig. 2). We defined the *effective monomer* as a hypothetical structural unit, comprising all types of monomeric units with their respective mole fractions, as described in detail in Section S4 (Eqs. 4 and S20). For example, the effective monomer of the PACIS-based copolymer in our simulations had a composition $PISC_{0.08}$-$PACIS_{0.71}$-$PI_{0.21}$ (cf. Table S2). Such a definition enabled us to compare the potentiometric titration and the cpH simulation data, where the simulated chains were shorter and had a fixed monomer sequence and chain length, whereas the experimental samples were polydisperse and their sequence of various monomeric units was random. As a result of this definition, we did not observe plateaus at integer values of Z_m^{eff}, as expected in simpler molecules or homopolymers. In addition, the value of the effective acidity constant pK_a^{eff} did not correspond to $Z_m^{eff} = n + 0.5e$ values, where n is an integer number. Therefore, the pK_a^{eff} value of copolymers with such a composition is difficult to determine precrisely for potentiometric titration measurements. However, in cpH simulations, we can directly measure the ionization states of individual groups, so we can also determine their pK_a^{eff} values by fitting the simulation titration data to Hill's equation (cf. Section S6 in the Supporting Information), as shown in Fig. 2.

Fig. 2B shows the net charge of the PISC-based copolymer, which was synthesized first. It has only two monomeric units: PISC and PI. From those, only PISC units feature ionizable groups: amine (NH_2), carboxylic acid (COOH) and sulfonic acid (SO_3^-). The SO_3^- groups are strongly acidic and, as such, negatively charged over the whole pH range, shifting Z_m^{eff} to negative values. For the COOH groups, the cpH simulations suggested a small deviation from the ideal HH behavior $\Delta pK_a^{eff} = pK_a^{eff} - pK_a = -0.14$. The potentiometric titration data also suggested a small ΔpK_a^{eff} for COOH, but in this range, the cpH simulation results slightly deviated from the experimental curve. For NH_2, the simulations predicted a significant shift $\Delta pK_a^{eff} = 1.21$ from the ideal HH baseline, whereas the potentiometric measurements remained close to the baseline. This result suggests that specific interactions, missing in our computer simulations, could have an important contribution to the protonation energy of the amine group.

Fig. 2C shows the net charge of the PACIS-based copolymer which has three different monomeric units: zwitterionic PACIS, containing NH_2 and COOH groups; neutral PI and a minor fraction of anionic PISC, containing NH_2, COOH and SO_3^- groups, as depicted in Fig. 1. The molar fraction of each of the monomeric units is reported in Table S1 in the Supporting Information. The cpH simulation predicts a moderate negative shift $pK_a^{eff} = -0.70$ for COOH (Fig. 2F) due to the favorable electrostatic interaction between the charged COO^- and NH_3^+ groups. This shift is consistent with the measurements from potentiometric titration, which also features a negative ΔpK_a^{eff} (Fig. 2C). However, we observed significant deviations between simulations and experiments at basic pH values, corresponding to the ionization of the NH_2 group. Again, computer simulations predicted a positive $\Delta pK_a^{eff} = 0.57$ whereas the potentiometric titration was slightly negatively shifted from the HH baseline.

We performed an additional set of cpH simulations to assess whether discrepancies between our experiments and simulations could be attributed to hydrophobic interactions due to the PI monomeric units and methyl groups in the PACIS and PISC units. In these cpH simulations, we replaced the purely repulsive WCA potential by attractive LJ interactions between these groups. We varied the strength of this interaction by the depth of the potential well. These attractive interactions shrunk the copolymer chain, as evidenced by the significantly lower values of the radius of gyration (cf. Section S4 in Supporting Information). However, the variation of hydrophobicity did not significantly affect the degree of ionization predicted by our computer simulations, as shown in Fig. 2, most likely because our polymer models are flexible and able to relocate their charged groups to favor electrostatics, even when the polymer chain collapses. Based on these observations, molecular interactions beyond simplified descriptions of our coarse-grained model are necessary to capture specific chemistry causing the deviations between simulations and experiments, which we observed at basic pH values.

Furthermore, our model considered just a single chain. In an ensemble of many chains, attractive hydrophobic interactions may lead to copolymer aggregation, affecting both the net charge and anticoagulant properties of the copolymers. The structure and size of such macromolecular aggregates can be kinetically driven but is thus beyond the current capabilities of our equilibrium simulations. Therefore, we used scattering techniques to detect aggregates in our copolymer samples, as described in the following section.

3.3. PISC- and PACIS-based copolymers form fractal-like aggregates in solution

By measuring Small Angle X-ray Scattering (SAXS) and Static Light Scattering (SLS), we examined the aggregation of our copolymers under acidic (A), neutral (N) and basic (B) conditions. To ensure constant ionic strength, we dissolved the polymers in 0.1 M HCl, deionized water with 0.1 M NaCl, and in 0.1 M NaOH. We were unable to measure SAXS for all samples due to the limited availability of the instrument time. For this reason, we focused on polymers sourced from the natural rubber PI. The corresping scattering curves are shown in Fig. 3.

The scattering curves were fitted by a model that describes particle shape by the Gaussian coil factor, $P_{Gauss}(q)$ and attractive interactions between particles (aggregation) by the mass fractal structure factor with an exponential cut-off, $S_{Exp}(q)$:

$$I(q) = I_0 P_{Gauss}(q) S_{Exp}(q) \tag{8}$$

where I_0 is the forward scattering intensity for $S_{Exp} = 1$ and

$$P_{Gauss}(q) = 2\frac{\exp\left(-q^2R_g^2\right) + q^2R_g^2 - 1}{q^4R_g^4} \tag{9}$$

$$S_{Exp}(q) = 1 + \frac{D\Gamma(D-1)\sin([D-1]\arctan[q\xi])}{(qr_0)^D\left[1+\frac{1}{q^2\xi^2}\right]^{\frac{D-1}{2}}} \tag{10}$$

Here, R_g stands for the radius of gyration of the Gaussian coil; ξ for the cut-off length of fractal correlations, related to the size of the aggregates; D, for the mass fractal dimension of the aggregate; r_0, for the characteristic dimension of individual scattering objects in the aggregate (that is, polymer chains); and $\Gamma(x)$, for the gamma function.

This model describes a hierarchical organization of local structures (lone coils) and fractal aggregates. At high q values (short length scales), we observe the scattering of individual Gaussian coils. At low q values

(longer length scales), we observe the scattering from the aggregates. For both PISC- and PACIS-based copolymers, the fractal dimension D was set to $D = 2.5$, which is the limit for dilute solutions and reaction-limited cluster aggregation (RLCA) [52]. The RLCA model assumes that particles collide frequently, but not every collision leads to aggregation. As a result, the aggregates formed by the RLCA mechanism are more compact than aggregates formed by a diffusion-limited mechanism.

In Fig. 3A and B, the model fits the SLS and SAXS scattering curves of both PISC- and PACIS-based copolymers. Knowing the chemical structure of the polymers, we hypothesize that the PI units form compact domains, separated by more loose structures containing the ionic PISC and PACIS units. In Fig. 3B, the PACIS_NR_N curve does not plateau, indicating that the aggregates are too large to reach their Guinier regime in the observed q range. Fitting the curve to the used model, thus, cannot provide the correlation length. (Since for $\xi \to \infty$ and $q \to 0$, $S_{Exp}(q) \propto q^{-D}$, the fit yields only the fractal dimension D from the power-law regime in the low q region).

In most cases, the fit (Table 2) yielded a correlation length on the order of tens of nm, which was significantly greater than the radius of gyration (2–4 nm). This supports our hypothesis that our polymers formed small domains of hydrophobic units, connected by loose coils composed mostly of hydrophilic segments. The only exception to this rule was PISC_NR A, where the fits yielded similar values of both R_g and ξ. Moreover, these values were affected by the solution pH. PISC is negatively charged over most of the pH range but becomes neutral at strongly acidic conditions (Fig. 3B). In contrast, PACIS is weakly positively charged under strongly acidic conditions but becomes uncharged close to the neutral pH and strongly negatively charged under basic conditions.

To complement the static scattering, the aggregates were also studied by Dynamic Light Scattering (DLS). DLS measurements of polyelectrolyte solutions often reveal multiple diffusive modes: a fast mode from free ions or single polymer chains, an intermediate mode related to segmental motion or transient interchain interactions, and a slow mode corresponding to multichain aggregates. These modes may occur simultaneously, but their identification is challenging as DLS data are intensity-weighted and dominated by larger scattering species, which can obscure less abundant or smaller components.[53] Unsurprisingly, our DLS measurements show multimodal distributions of intensity-weighted hydrodynamic radii, in contrast to monomodal number-weighted distributions for both PISC-(Fig. 3D, 3E) and PACIS-based copolymers (Fig. 3G, 3H). Therefore, most of the polymers are dissolved as single chains, whereas the large aggregates account for only a small fraction of the whole sample.

From the slope of the relation between the inverse Rayleigh ratio and the scattering vector on logarithmic scales for PISC- (Fig. 3F) and PACIS-based copolymers (Fig. 3I), we determined the fractal dimension D of the aggregates. The linearity of these plots across the measured q-range suggests self-similar scattering and the dominance of a single aggregate type without hierarchical organization. Surprisingly, for PACIS-based copolymers, the shortest chains formed large aggregates, most likely due to their rigidity and lack of conformational stability. Conversely, the longer polymer chains formed loose aggregates because their intramolecular flexibility improves their stability.

Table 2
SLS-SAXS fitting parameters (forward scattering intensity at $S_{Exp} = 1$, I_0, radius of gyration R_g, cut-off length ξ and characteristic dimension of individual scattering objects $_0$).

	I_0(a.u.)	R_g(nm)	ξ(nm)	r_0(nm)
PISC_NR A	13.3	10	18	0.1
PISC_NR N	2.76	3	71	8
PISC_NR B	2.67	2	55	5
PACIS_NR A	2.85	4	17	11
PACIS_NR N	2.33	3	∞	8
PACIS_NR B	1.41	2	61	4

3.4. PISC- and PACIS-based copolymers show anticoagulant activity and biocompatibility in vitro

As an anticoagulant, heparin enhances antithrombin activity. Antithrombin inactivates clotting factors, such as thrombin and factor Xa, thus prolonging the activated partial thromboplastin time (aPTT). Clinically, aPTT is the most commonly used parameter for assessing the state of the intrinsic coagulation pathway. This parameter is expressed as the percentage of the corresponding time of a vehicle, that is, the solution or buffer in which the cells are suspended for the assay.

We measured the aPTT of PISC_7K, PISC_NR, PISC_75K, PACIS_7K, PACIS_NR and PACIS_75K in human plasma, using heparin sodium salt from porcine intestinal mucosa as a positive control. The aPTT was expressed as a percentage relative to the coagulation time of buffer-treated control samples (i.e., a vessel without an active compound). The results indicated that the anticoagulant efficacy of these copolymers increases with chain length (Fig. 4A). For example, when adding 25 µl of 100 µg/mL polymer solution (the final concentration of the polymer in the sample solution: 7.69 µg/L), PISC_7K and PISC_75K prolonged the coagulation time by more than 500% and by nearly 1000%, respectively. In contrast, the sample treated with the positive control (heparin) at the same concentration did not clot after 24 h.

Anticoagulant activity was also strongly correlated with polymer concentration (Fig. 4B, Section S8 in Supporting Information). aPTT increased exponentially with polymer concentration for both PISC- and PACIS-based copolymers, regardless of chain length. Samples treated with 500 and 1000 µg/mL of copolymers did not clot after 24 h. This positive effect of polymer concentration on aPTT may be explained by the inherent increase in functional groups involved in anticoagulant activity.

Broadly speaking, PISC-based copolymers led to longer coagulation times than PACIS-based copolymers. At lower concentrations (5 and 10 µg/mL), their activity was only slightly above 100% vehicle, preventing any comparison. But at higher concentrations (50 and 100 µg/mL), PISC-based copolymers significantly outperformed their PACIS-based counterparts with the same chain length, except for copolymers with 75 K chains, which showed virtually identical values. This difference in anticoagulant activity reflects the higher density of negative charges of PISC-based copolymers. Combined, these findings confirm that the net negative charge of heparin mimetics is the determining factor of anticoagulant activity [54–56].

To assess the biocompatibility of the polymeric anticoagulants, we performed dose–response tests in HEK-293 (immortalized epithelial cell line derived from human embryonic kidney cells), CCD-841 (colonocytes from a healthy donor), Cal-148 (human breast adenocarcinoma), Cal-51 (human breast adenocarcinoma), MDA-MB-231 cell lines (human breast adenocarcinoma) and MV4-11(human acute myeloid leukemia) (Fig. 4C). The cells were treated with a wide range of concentrations (starting concentration 316 µg/mL; 3.16 × dilution factor) of PISC- and PACIS-based copolymers with different chain lengths to assess cell proliferation inhibition. Cell proliferation inhibition was expressed as a percentage of control, samples treated with cell culture media, where negative values indicate cell growth stimulation, and positive – growth inhibition.

In these *in vitro* tests, the polymers stimulated cell growth up to 100 µg/mL concentration (especially on MDA-MB-231) and exhibited moderate cell growth inhibition at 316 µg/mL (Fig. 4C1, 4C2, 4C3, 4C4, 4C5, 4C6). We were able to calculate the IC_{50} parameter only for PISC_7K in Cal-148 and MV-4–11 (IC_{50} = 195 µg/mL and 268 µg/mL, respectively), PACIS_75K in Cal-51 and MV-4–11 (IC_{50} = 310 µg/mL and 34.7 µg/mL, respectively), PACIS_7K in MV-4–11, HEK-293, and CCD-841 (IC_{50} = 204 µg/mL, 60.59 µg/mL and 90.91 µg/mL, respectively) and PISC_75K in MV-4–11 (266 µg/mL). Nevertheless, the mimetics showed

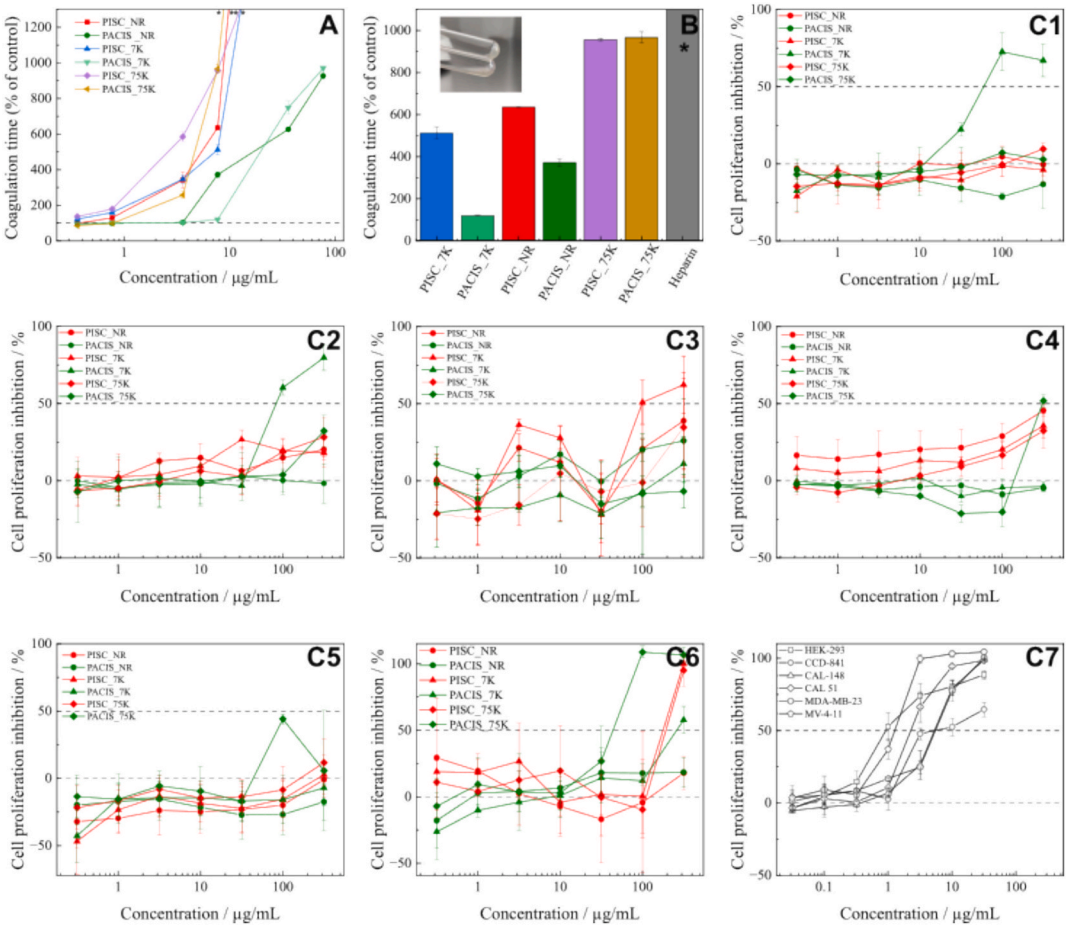

Fig. 4. Heparin mimetics display anticoagulant activity without causing cytotoxicity. Antithrombotic effects of PISC- and PACIS-based polymers. (**A**) Clotting time using activated partial thromboplastin time (aPPT) *in vitro* of PISC_NR, PACIS_NR, PISC_7K, PACIS_7K, PISC_75K, PACIS_75K after adding 25 µl of solutions with concentrations ranging from 0.36 to 77 µg/mL, (**B**) aPPT of 7.7 µg/mL PISC_7K, PACIS_7K, PISC_NR, PACIS_NR, PISC_75K, PACIS_75K and heparin from porcine intestinal mucosa (used as a standard), where the asterisk symbolizes the value exceeding the plot scale. Inset: photograph of unclotted human blood plasma (bottom vial) and readily formed stable fibrin clot (top vial). Dose-response tests **(C)** presented as variations of HEK-293 **(C1)**, CCD-841 **(C2)** Cal-148 **(C3)**, Cal-51 **(C4)**, MDA-MB-231 **(C5)**, and MV-4–11 **(C6)** cell proliferation inhibition as a function of copolymer concentration for PISC_NR, PACIS_NR, PISC_7K, PACIS_7K, PISC_75K and PACIS_75K, and cell proliferation inhibition of these cell lines as a function of cisplatin concentration **(C7)**.

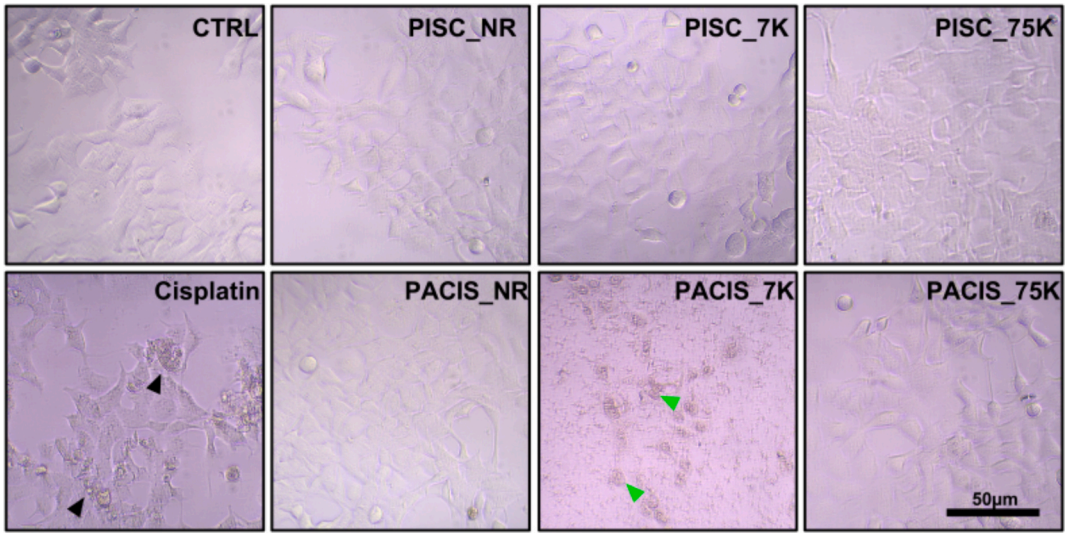

Fig. 5. HEK-293 cell images acquired in brightfield mode after 72 hr of treatment with culture medium (CTRL), 1 µg/mL of cisplatin (Cisplatin) or 100 µg/mL of the heparin mimetics. Black arrowheads indicate apoptotic cells, green arrowheads indicate plausibly necrotic cells. (To interpret references to color in this figure legend, the reader should refer to the web version of this article.)

significantly lower cytotoxicity ($IC50^{HEK-293}_{cisplatin}$ = 1.25μg/mL, $IC50^{CCD-841}_{cisplatin}$ = 2.84μg/mL, $IC50^{Cal-148}_{cisplatin}$ = 5.26μg/mL, $IC50^{Cal-51}_{cisplatin}$ = 2.34μg/mL, $IC50^{MDA-MB-231}_{cisplatin}$ = 6.32μg/mL, $IC50^{MV-4-11}_{cisplatin}$ = 1.25μg/mL) than cisplatin (Fig. 4C7)

In some polymers, we observed a trophic effect, which might have derived from the ability of heparin mimetics to activate trophic receptors, such as fibroblast growth factor receptors (FGFRs), or other heparin-binding growth factor pathways. [57,58] The negatively charged functional groups of the heparin-mimicking polymers and their spatial arrangement along the polymer chain promote interactions with the positively charged residues on the surface of target proteins, as with natural heparin interactions. This behavior modulates their activity and may stimulate cell proliferation. Although this effect might signify hormesis, our current data and the statistical analyses are too limited to draw firm conclusions about its underlying mechanisms.

Visual examination of the HEK-293 cells 72hrs after treatment confirmed the lack of any observable influence of heparin mimetics on the morphology of HEK-293 cells, except for PACIS_7K, which showed large amounts of debris, along with dead, detached cell,likely resulting from necrosis. (Fig. 5) Further studies should be conducted to confirm the underlying molecular mechanisms of cell death.

Toxicity was assessed using the hemolysis assay in which hRBCs were treated with PISC- and PACIS-based copolymer solutions (Section S7 in the Supporting Information). Hemolysis was expressed as the concentration of the active agent at 50% hRBC lysis (EC_{50}). The PACIS_NR- and PISC_NR-based copolymers reached EC_{50} of 379 and 1565 μg/mL, respectively. Both studied polymers can be considered non-toxic, underlining their potential for clinical applications in anticoagulation therapy.

Although these results highlight the potential of PISC- and PACIS-based copolymers as functional heparin mimetics, with their high anticoagulant activity and low toxicity *in vitro*, the trophic activity of these synthetic alternatives would require further testing to understand their detailed mechanism. Future research will focus on fine-tuning the copolymer architecture to enhance its bioactivity and specificity as these considerations are essential to developing safe, controllable, and highly active heparin alternatives.

4. Conclusions

Copolymers derived from polyisoprene (PI) from both natural rubber and anionic polymerization can be used as effective anticoagulants with potential applications as synthetic heparin replacements. More specifically, sodium poly((sulfamate-carboxylate)isoprene) (PISC) and poly ((amino-carboxylate) isoprene (PACIS) can be prepared by a post-polymerization reaction to contain not only sulfonate groups for high charge density but also weakly acidic and basic groups on adjacent carbons for tuning their net charge in the biological pH range, while simultaneously maintaining their solubility and anticoagulation activity. The flexibility of the polymer chain and high sulfation degree enable interactions with coagulation factors, thereby preventing fibrin clot formation. Their heparin-mimicking activity derives from their high charge density and number of ionizable groups, as shown in our study combining experimental methods with molecular simulations. Because both PISC- and PACIS-based copolymers contain 20% unmodified hydrophobic PI units, they form fractal aggregates in aqueous solutions, whose structure depends on the pH and polymer architecture. Increasing chain length decreases aggregate size because intramolecular flexibility improves stability. In spite of some aggregation, all copolymer samples show significant anticoagulant activity and biocompatibility *in vitro*. They promote cell proliferation at concentrations of up to 100 μg/mL. These findings highlight the potential of these copolymers as tunable, biocompatible materials for anticoagulation therapy and, therefore, as alternatives to heparin.

CRediT authorship contribution statement

Katarzyna Byś: Writing – review & editing, Writing – original draft, Visualization, Validation, Project administration, Methodology, Investigation, Funding acquisition, Formal analysis, Data curation, Conceptualization. **Pablo M. Blanco:** Writing – review & editing, Writing – original draft, Visualization, Validation, Software, Methodology, Investigation, Formal analysis, Data curation. **Krzysztof Fink:** Validation, Methodology, Investigation, Formal analysis, Data curation. **Mateusz Psurski:** Validation, Methodology, Investigation, Formal analysis, Data curation. **Honorata Zachary:** Methodology, Investigation. **Miroslav Štěpánek:** Writing – review & editing, Resources, Funding acquisition. **Peter Košovan:** Writing – review & editing, Writing – original draft, Validation, Supervision, Software, Methodology, Investigation, Funding acquisition, Formal analysis, Data curation. **Mariusz Uchman:** Writing – review & editing, Writing – original draft, Validation, Supervision, Resources, Project administration, Funding acquisition, Formal analysis, Conceptualization.

Declaration of competing interest

The authors declare that they have no known competing financial interests or personal relationships that could have appeared to influence the work reported in this paper.

Acknowledgements

The authors acknowledge the Grant Agency of Charles University (GAUK) for funding this study through GAUK 405122. PK and MŠ acknowledge financial support from the Czech Ministry of Education, Youth and Sports, project No. LUAUS25140 and Operational Programme Research, Development and Education: “Excellent Research Teams”, project no. CZ.02.1.01/0.0/0.0/15_003/0000417-CUCAM respectively. We acknowledge CMS-Biocev (”Biophysical techniques, Crystallization, Diffraction, Structural mass spectrometry”) of CIISB, Instruct-CZ Center, supported by MEYS CR (LM2023042) and CZ.02.1.01/0.0/0.0/18 046/0015974. The authors would like to thank doc. Ivana Šloufová for the FTIR analysis, Dr. O. Kočková for the elemental analysis, Dr. B. Strachota for the thermogravimetric analysis, Prof. B. Mossety-Leszczak for the DSC measurements, Dr. J. Stránský for assistance in SAXS measurements, and BSc. P. Šimková for the SLS measurements. The authors would like to thank Dr. A. Strachota for the insightful discussions and providing his expertise in synthesis. The authors also thank Dr. Carlos V. Melo for editing the manuscript.

Appendix A. Supplementary data

Supplementary data to this article can be found online at https://doi.org/10.1016/j.eurpolymj.2025.114440.

Data availability

Data will be made available on request.

References

[1] T. Vos, et al., Global burden of 369 diseases and injuries in 204 countries and territories, 1990–2019: a systematic analysis for the Global Burden of Disease Study 2019, Lancet 396 (10258) (2020) 1204–1222, https://doi.org/10.1016/S0140-6736(20)30925-9.

[2] D. Jiménez, et al., Hospital volume and outcomes for acute pulmonary embolism: Multinational population based cohort study, The BMJ 366 (2019), https://doi.org/10.1136/bmj.l4416.

[3] A. Abdulla, W.M. Davis, N. Ratnaweera, E. Szefer, B. Ballantyne Scott, A.Y.Y. Lee, A Meta-Analysis of Case Fatality rates of Recurrent Venous Thromboembolism and Major Bleeding in patients with Cancer, Thromb. Haemost. 120 (4) (2020) 702–713, https://doi.org/10.1055/s-0040-1708481.

[4] D. Wichmann, et al., Autopsy findings and venous thromboembolism in patients with COVID-19: a prospective cohort study, Ann. Intern. Med. 173 (4) (2020) 268–277, https://doi.org/10.7326/M20-2003.

[5] J. Hogwood, B. Mulloy, R. Lever, E. Gray, C.P. Page, Pharmacology of Heparin and Related drugs: an Update, Pharmacol. Rev. 75 (2) (2023) 328–379, https://doi.org/10.1124/pharmrev.122.000684.

[6] J. Hirsh, S.S. Anand, J.L. Halperin, V. Fuster, Guide to Anticoagulant Therapy: Heparin a Statement for Healthcare professionals from the American Heart Association [Online]. Available: http://www.circulationaha.org, 2001.

[7] J. Amiral and A. marie Vissac, "Role of Heparin-Dependent Antigens in Immune Heparin-Induced Thrombocytopenia," in *Heparin-Induced Thrombocytopenia*, 2007, 131–148. 10.3109/9781420045093.005.

[8] L.E. Vincent, et al., Association of Changes in Antithrombin activity over Time with Responsiveness to Enoxaparin Prophylaxis and risk of Trauma-Related Venous Thromboembolism, J. Am. Med. Assoc.Surg 157 (8) (2022) 713–721, https://doi.org/10.1001/jamasurg.2022.2214.

[9] I. Pabinger, J. Thaler, How I treat patients with hereditary antithrombin deficiency, Blood 134 (26) (2019) 2346–2353, https://doi.org/10.1182/blood.2019002927.

[10] A. Al Nahain, V. Ignjatovic, P. Monagle, J. Tsanaktsidis, V. Ferro, Heparin mimetics with anticoagulant activity, Med. Res. Rev. 38 (5) (2018) 1582–1613, https://doi.org/10.1002/med.21489.

[11] H. Bussey, J. L. Francis, H. C. Group, "Heparin Overview and issues," *Pharmacotherapy: the Journal of Human Pharmacology and Drug*, Therapy 24 (8P2) (2004) 103S–S107, https://doi.org/10.1592/phco.24.12.103S.36109.

[12] L. Ma, et al., In vitro and in vivo anticoagulant activity of heparin-like biomacromolecules and the mechanism analysis for heparin-mimicking activity, Int J Biol Macromol 122 (2019) 784–792, https://doi.org/10.1016/j.ijbiomac.2018.11.011.

[13] X. Chen, et al., Sulfonate groups and Saccharides as Essential Structural elements in Heparin-Mimicking Polymers used as Surface Modifiers: Optimization of Relative Contents for Antithrombogenic Properties, ACS Appl Mater Interfaces 10 (1) (2018) 1440–1449, https://doi.org/10.1021/acsami.7b16723.

[14] W. Sun, et al., Vascular cell responses to silicone surfaces grafted with heparin-like polymers: surface chemical composition vs. topographic patterning, J. Mater. Chem. B 8 (39) (2020) 9151–9161, https://doi.org/10.1039/D0TB01000F.

[15] S.J. Paluck, T.H. Nguyen, H.D. Maynard, Heparin-Mimicking Polymers: Synthesis and Biological applications, Biomacromolecules 17 (11) (2016) 3417–3440, https://doi.org/10.1021/acs.biomac.6b01147.

[16] M. Hoffmann, N.L. Snyder, L. Hartmann, Polymers inspired by Heparin and Heparan Sulfate for Viral Targeting, Macromolecules 55 (18) (2022) 7957–7973, https://doi.org/10.1021/acs.macromol.2c00675.

[17] R.M. Maaroufi, M. Jozefowicz, J. Tapon-Bretaudière, A.-M. Fischer, Mechanism of thrombin inhibition by antithrombin and heparin cofactor II in the presence of heparin, Biomaterials 18 (3) (1997) 203–211, https://doi.org/10.1016/S0142-9612(96)00125-1.

[18] B. Kalaska, et al., Anticoagulant Properties of Poly(sodium 2-(acrylamido)-2-methylpropanesulfonate)-based Di- and Triblock Polymers, Biomacromolecules 19 (7) (Jul. 2018) 3104–3118, https://doi.org/10.1021/acs.biomac.8b00691.

[19] A. Al Nahain, V. Ignjatovic, P. Monagle, J. Tsanaktsidis, G. Vamvounis, V. Ferro, Anticoagulant Heparin Mimetics via RAFT Polymerization, Biomacromolecules 21 (2) (2020) 1009–1021, https://doi.org/10.1021/acs.biomac.9b01688.

[20] H. Wang, et al., Artificial Extracellular Matrix Composed of Heparin-Mimicking Polymers for Efficient Anticoagulation and Promotion of Endothelial Cell Proliferation, ACS Appl Mater Interfaces 14 (44) (2022) 50142–50151, https://doi.org/10.1021/acsami.2c13892.

[21] M. Uchman, et al., Multicompartment Nanoparticles formed by a Heparin-Mimicking Block Terpolymer in Aqueous Solutions, Macromolecules 42 (15) (2009) 5605–5613, https://doi.org/10.1021/ma9008115.

[22] L. Wang, T. Qiu, F. Xu, L. Zhang, C. Zhang, W. Ye, Fabricate heparin-mimic thin gel layers for vascular cell selective regulation using 5-hydroxydopamine cross-linked chitosan and sulfonated polymers, Int J Biol Macromol 311 (2025) 144027, https://doi.org/10.1016/j.ijbiomac.2025.144027.

[23] D. Fan, X. Liu, H. Chen, Endothelium-Mimicking Materials: a 'rising Star' for Antithrombosis, ACS Appl Mater Interfaces 16 (40) (2024) 53343–53371, https://doi.org/10.1021/acsami.4c12117.

[24] P. Nair, R. Trivedi, P. Hu, Y. Zhang, A.M. Merchant, Low-molecular weight vs. unfractionated heparin for prevention of venous thromboembolism in general surgery: a meta-analysis, Updates Surg 73 (1) (2021) 75–83, https://doi.org/10.1007/s13304-020-00872-w.

[25] Z. Iqbal, S. Sadaf, Commercial Low Molecular Weight Heparins — Patent Ecosystem and Technology Paradigm for Quality Characterization, J. Pharm.Innov 18 (2) (2023) 803–835, https://doi.org/10.1007/s12247-022-09665-7.

[26] J. Hirsh, Low-Molecular-Weight Heparin, Circulation 98 (15) (1998) 1575–1582, https://doi.org/10.1161/01.CIR.98.15.1575.

[27] M. Hogan, J.S. Berger, Heparin-induced thrombocytopenia (HIT): Review of incidence, diagnosis, and management, Vasc. Med. 25 (2) (2020) 160–173, https://doi.org/10.1177/1358863X19898253.

[28] T. E. Jones, S. Brian J, and J. F. and Polasek, "Pharmacoeconomics of low-molecular-weight heparins: limitations of studies comparing them to unfractionated heparin," *Expert Opin Pharmacother*, 5(9), 1887–1897, 2004, 10.1517/14656566.5.9.1887.

[29] C.C. Heuck, U. Schiele, D. Horn, D. Fronda, E. Ritz, The role of surface charge on the accelerating action of heparin on the antithrombin III-inhibited activity of alpha-thrombin, J. Biol. Chem. 260 (8) (1985) 4598–4603, https://doi.org/10.1016/S0021-9258(18)89113-X.

[30] Y. Sang, M. Roest, B. de Laat, P.G. de Groot, D. Huskens, Interplay between platelets and coagulation, Blood Rev. 46 (2021) 100733, https://doi.org/10.1016/j.blre.2020.100733.

[31] M. Stornes, P.M. Blanco, R.S. Dias, Polyelectrolyte-nanoparticle mutual charge regulation and its influence on their complexation, Colloids Surf. APhysicochem Eng Asp 628 (2021) 127258, https://doi.org/10.1016/j.colsurfa.2021.127258.

[32] R. Lunkad, et al., Quantitative prediction of charge regulation in oligopeptides, Mol Syst Des Eng 6 (2) (2021) 122–131, https://doi.org/10.1039/D0ME00147C.

[33] R. Lunkad, A. Murmiliuk, Z. Tošner, M. Štěpánek, and P. Košovan, "Role of pKA in Charge Regulation and Conformation of Various Peptide Sequences," *Polymers (Basel)*, 13(2), 2021, 10.3390/polym13020214.

[34] R. Lunkad, et al., Simulations and Potentiometric Titrations Enable Reliable Determination of Effective pKa Values of Various Polyzwitterions, Macromolecules 55 (17) (2022) 7775–7784, https://doi.org/10.1021/acs.macromol.2c01121.

[35] S. Pispas, Double hydrophilic block copolymers of sodium(2-sulfamate-3-carboxylate)isoprene and ethylene oxide, J Polym Sci A Polym Chem 44 (1) (2006) 606–613, https://doi.org/10.1002/pola.21196.

[36] L. Van Der Does, T. Beugeling, P.E. Froehling, A. Bantjes, Synthetic polymers with anticoagulant activity, J. Polym. Sci., Polym. Symp. 66 (1) (1979) 337–348, https://doi.org/10.1002/polc.5070660131.

[37] S. Jana, et al., Individual and simultaneous encapsulation and delivery of incompatible dyes in biocompatible multicompartment terpolymer micelles, Eur Polym J 218 (2024) 113344, https://doi.org/10.1016/j.eurpolymj.2024.113344.

[38] M.N. Leiske, B.G. De Geest, R. Hoogenboom, Impact of the polymer backbone chemistry on interactions of amino-acid-derived zwitterionic polymers with cells, Bioact Mater 24 (2023) 524–534, https://doi.org/10.1016/j.bioactmat.2023.01.005.

[39] A. Traeger, M.N. Leiske, The whole is Greater than the Sum of its Parts – challenges and Perspectives in Polyelectrolytes, Biomacromolecules 26 (1) (2025) 5–32, https://doi.org/10.1021/acs.biomac.4c01061.

[40] S. Förster, M. Schmidt, M. Antonietti, Static and dynamic light scattering by aqueous polyelectrolyte solutions: effect of molecular weight, charge density and added salt, Polymer (guildf) 31 (5) (1990) 781–792, https://doi.org/10.1016/0032-3861(90)90036-X.

[41] D. Beyer, P.M. Blanco, J. Landsgesell, P. Košovan, C. Holm, How to Correct Erroneous Symmetry-breaking in Coarse-Grained constant-pH Simulations, J Chem Theory Comput 21 (3) (2025) 1396–1404, https://doi.org/10.1021/acs.jctc.4c01010.

[42] R. Weeber *et al.*, "ESPResSo, a Versatile Open-Source Software Package for Simulating Soft Matter Systems," 2023. 10.1016/B978-0-12-821978-2.00103-3.

[43] D. Beyer, et al., pyMBE: the Python-based molecule builder for ESPResSo, J Chem Phys 161 (2) (2024) 022502, https://doi.org/10.1063/5.0216389.

[44] T. Mosmann, Rapid colorimetric assay for cellular growth and survival: Application to proliferation and cytotoxicity assays, J Immunol Methods 65 (1) (1983) 55–63, https://doi.org/10.1016/0022-1759(83)90303-4.

[45] P. Skehan, et al., New Colorimetric Cytotoxicity Assay for Anticancer-Drug Screening, J. Natl Cancer Inst. 82 (1990) 1107–1112, https://doi.org/10.1093/jnci/82.13.1107.

[46] F. Chen, J. Qian, Studies on the thermal degradation of cis-1,4-polyisoprene, Fuel 81 (16) (2002) 2071–2077, https://doi.org/10.1016/S0016-2361(02)00147-3.

[47] Y. Kinoshita, et al., Synthetic polymer sulphonated polyisoprene as a universal anticoagulant for laboratory testing, J Clin Lab Anal 14 (4) (2000) 180–187, https://doi.org/10.1002/1098-2825(2000)14:4<180::AID-JCLA7>3.0.CO;2-E.

[48] J. De Breuck, et al., Amino-Acid-Derived Anionic Polyacrylamides with Tailored Hydrophobicity–Physicochemical Properties and Cellular Interactions, ACS Polymers Au 4 (3) (2024) 222–234, https://doi.org/10.1021/acspolymersau.3c00048.

[49] E. M. Pearce, "Kirk-Othmer encyclopedia of chemical technology, 3rd ed., I, Wiley-Interscience, New York, 1978.," *Journal of Polymer Science: Polymer Letters Edition*, 16(5), 248, 1978, 10.1002/pol.1978.130160508.

[50] B. Tonpheng, O. Andersson, Crosslinking, thermal properties and relaxation behaviour of polyisoprene under high-pressure, Eur Polym J 44 (9) (2008) 2865–2873, https://doi.org/10.1016/j.eurpolymj.2008.07.010.

[51] P. M. Blanco, C. F. Narambuena, S. Madurga, F. Mas, and J. L. Garcés, "Unusual Aspects of Charge Regulation in Flexible Weak Polyelectrolytes," *Polymers (Basel)*, 15(12), 2023, 10.3390/polym15122680.

[52] S. Jungblut, J.-O. Joswig, A. Eychmüller, Diffusion- and reaction-limited cluster aggregation revisited, PCCP 21 (10) (2019) 5723–5729, https://doi.org/10.1039/C9CP00549H.

[53] M. Sedlák, What can Be Seen by Static and Dynamic Light Scattering in Polyelectrolyte Solutions and Mixtures? Langmuir 15 (12) (1999) 4045–4051, https://doi.org/10.1021/la981189j.

[54] X. Wang, M.K. Hadi, J. Niu, Q. Zhou, F. Ran, Anticoagulant Macromolecules, Macromolecules 56 (12) (2023) 4387–4430, https://doi.org/10.1021/acs.macromol.2c02501.

[55] F. Ran, et al., Synthesized negatively charged macromolecules (NCMs) for the surface modification of anticoagulant membrane biomaterials, Int J Biol Macromol 55 (2013) 269–275, https://doi.org/10.1016/j.ijbiomac.2013.01.014.

[56] F. Lin, et al., Porous Polymers as Universal Reversal Agents for Heparin Anticoagulants through an Inclusion–Sequestration Mechanism, Adv. Mater. 34 (23) (2022) 2200549, https://doi.org/10.1002/adma.202200549.
[57] S.C. Griffiths, et al., Hedgehog-Interacting Protein is a multimodal antagonist of Hedgehog signalling, Nat Commun 12 (1) (2021) 7171, https://doi.org/10.1038/s41467-021-27475-2.
[58] J. Schlessinger, et al., Crystal Structure of a Ternary FGF-FGFR-Heparin complex reveals a dual Role for Heparin in FGFR Binding and Dimerization, Mol Cell 6 (3) (2000) 743–750, https://doi.org/10.1016/S1097-2765(00)00073-3.